Optical properties of tissues quantified by Fourier-transform light scattering

Huafeng Ding,[1] Freddy Nguyen,[2] Stephen A. Boppart,[2] and Gabriel Popescu[1,*]

[1]*Quantitative Light Imaging Laboratory, Beckman Institute for Advanced Science and Technology, University of Illinois at Urbana-Champaign, Urbana, Illinois 61801, USA*
[2]*Biophotonics Imaging Laboratory, Beckman Institute for Advanced Science and Technology, University of Illinois at Urbana-Champaign, Urbana, Illinois 61801, USA*
**Corresponding author: gpopescu@illinois.edu*

Received February 6, 2009; accepted March 2, 2009;
posted March 25, 2009 (Doc. ID 107291); published April 22, 2009

We employ Fourier-transform light scattering, a technique recently developed in our laboratory, to study the scattering properties of rat organ tissues. Using the knowledge of the complex field associated with high-resolution microscope images of tissue slices, we extracted the scattering mean-free path l_s and anisotropy factor g, which characterize the bulk tissue for three different rat organs. This "bottom up" approach to measuring tissue scattering parameters allows for predicting the wave transport phenomena within the organ of interest at a multitude of scales—from *organelle to organ* level. © 2009 Optical Society of America

OCIS codes: 290.5820, 170.3660, 170.6935, 170.0180, 180.3170.

Upon propagation through inhomogeneous media, optical fields undergo modifications in terms of irradiance, phase, spectrum, direction, polarization, and coherence, which can reveal information about the sample of interest. Light scattering by cells and tissues evolved as a dynamic area of study, especially because this type of investigation can potentially offer a noninvasive window into function and pathology [1–9]. Despite all these efforts, light-scattering-based techniques currently have limited use in the clinic. A great challenge is posed by the insufficient knowledge of the tissues's optical properties.

Recent *phase-sensitive* methods have been employed to directly extract the refractive index of cells and tissues [10]. These approaches have been extended further to three-dimensional (3D) reconstructions of cell refractive index [11,12]. Starting from the measured 3D refractive index distribution, the angular scattering has been retrieved via the Born approximation [13]. Based on diffraction phase microscopy (DPM) [14], we developed Fourier-transform light scattering (FTLS) as an experimental approach for studying inhomogeneous and dynamic media [15]. In FTLS the optical phase and amplitude of a coherent image field are quantified and propagated numerically to the scattering plane.

In this Letter, we use FTLS to extract quantitatively the scattering mean-free path l_s and anisotropy factor g from tissue slices of different organs. This direct measurement of tissue scattering parameters allows for predicting the wave transport phenomena within the organ of interest at a multitude of scales. Figure 1 depicts our experimental setup, presented in more detail previously [14]. Briefly, the fiber-coupled second harmonic of a diode-pumped Nd:YAG laser ($\lambda = 532$ nm) is collimated and used to illuminate the sample in transmission. At the sample plane, the laser beam is larger than a centimeter, with a total power of approximately 3 mW. An amplitude diffraction grating G (110 grooves/mm) is placed at the image plane. To establish a common-path Mach–Zehnder interferometer, a standard spatial filtering lens set L_1–L_2 (i.e., 4-f system) with focal lengths of 60 and 300 mm is used to select the two diffraction orders and generate the final interferogram at the CCD plane. The zeroth-order beam is low-pass filtered using a pinhole (25 μm diameter) at the spatial filter (SF) plane, which is the Fourier plane of L_1. Thus, at the CCD plane this zeroth-order beam approaches a uniform, i.e., reference, field. Simultaneously, the SF allows for passing the entire frequency content of the first diffraction-order beam and blocks all the other orders. The two beams propagate along a common optical path, significantly reducing the longitudinal phase noise. From a single CCD exposure, we obtain the spatially resolved phase and amplitude associated with the image field, $U(\mathbf{r}) = |U(\mathbf{r})| e^{i\phi(\mathbf{r})}$ [14].

Figures 2(a)–2(c) show examples of quantitative phase images associated with 5 μm tissue slices for three different organs from a rat, which were prepared according to a standard procedure under a protocol approved by the Institutional Animal Care and Use Committee at the University of Illinois at Urbana-Champaign. The scattered intensity for each slice is obtained by Fourier transforming the complex image field,

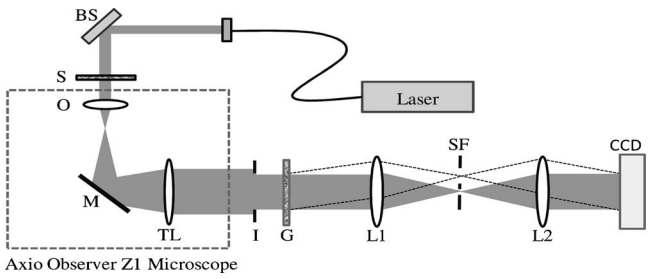

Fig. 1. Schematic of the FTLS setup. FC, fiber collimator; BS, beam splitter; S, sample; O, objective lens; M, mirror; TL, tube lens; I, iris; G, grating; SF, spatial filter; L1 and L2, lenses.

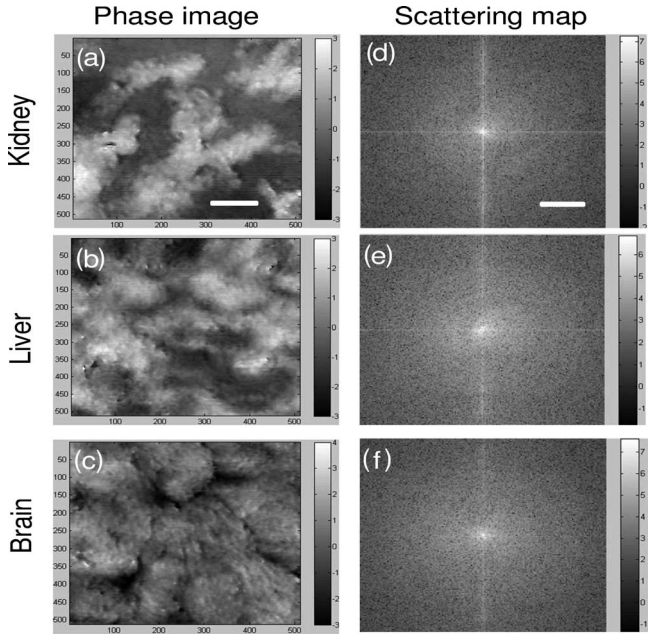

Fig. 2. (a)–(c) Examples of quantitative phase images (512×512 pixels) for rat kidney, liver, and brain, respectively. Scale bar shows 25 μm; (d)–(f) The scattering maps (logarithmic scale) associated with the phase images (a)–(c). Scale bar shows 0.14 rad.

$$\tilde{I}(\mathbf{q}) \propto \left| \int\int [|U(\mathbf{r})|e^{i\phi(\mathbf{r})}]e^{i\mathbf{q}\cdot\mathbf{r}}\mathrm{d}^2\mathbf{r} \right|^2. \quad (1)$$

In Eq. (1), $\mathbf{q}$ is the momentum transfer of modulus $q=(4\pi/\lambda)\sin(\theta/2)$, with θ as the scattering angle. The scattering maps associated with the phase images [Figs. 2(a)–2(c)] are shown in Figs. 2(d)–2(f).

The scattering mean-free path l_s was measured by quantifying the attenuation owing to scattering for each slice via the Lambert–Beer law, $l_s=-d/\ln[I(d)/I_0]$, where d is the thickness of the tissue, $I(d)$ is the irradiance of the unscattered light after transmission through the tissue, and I_0 is the total irradiance, i.e., the sum of the scattered and unscattered components. The unscattered intensity $I(d)$ is evaluated by integrating the angular scattering over the diffraction spot around the origin. The resulting l_s values for 20 samples for each organ from the same rat are summarized in Fig. 3(a). Ritz *et al.* [19] report much-larger values for l_s of pig liver. However, their wavelength is in the near-IR, which is expected to scatter less strongly than our green light. Parsa *et al.* [20], on the other hand, report $l_s=60$ μm at our wavelength by using the integrating sphere and diffusion model. This l_s value is a factor of ~4 larger than our values [Fig. 3(a)]. We believe that differences in sample preparation may explain this discrepancy.

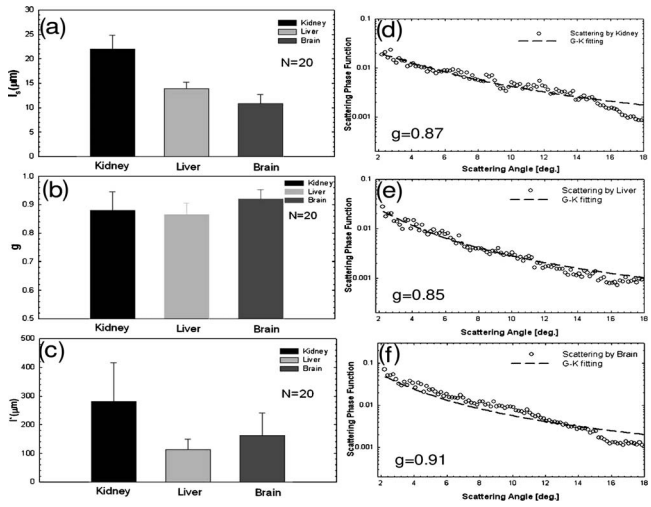

Fig. 3. FTLS measurements of the (a) scattering mean-free path l_s, (b) anisotropy factors, and (c) transport mean-free path for the three rat organs with 20 samples per group. The error bars correspond to the standard deviations ($N=20$). (d)–(f) The angular-scattering plots associated with the scattering maps in Figs. 2(d)–2(f). The dashed curves indicate fits with the GK phase function.

The anisotropy factor g is defined as the average cosine of the scattering angle,

$$g = \frac{\int_{-1}^{1} \cos(\theta)p[\cos(\theta)]\mathrm{d}[\cos(\theta)]}{\int_{-1}^{1} p[\cos(\theta)]\mathrm{d}[\cos(\theta)]}, \quad (2)$$

where p is the normalized angular scattering, i.e., the phase function. Note that since Eq. (1) applies to tissue slices of thickness $d<l_s$, it cannot be used directly in Eq. (2) to extract g since g values in this case will be thickness dependent. This is so because the calculation in Eq. (2) is defined over tissue of thickness $d=l_s$, which describes the average scattering properties of the tissue (i.e., independent of how the tissue is cut). Under the weakly scattering regime of interest here, this angular-scattering distribution p is obtained by propagating the complex field numerically through $N=l_s/d$ layers of $d=5$ μm thickness,

$$p(\mathbf{q}) \propto \left| \int\int [U(\mathbf{r})]^N e^{i\mathbf{q}\cdot\mathbf{r}}\mathrm{d}^2\mathbf{r} \right|^2. \quad (3)$$

Equation (3) applies to a slice of thickness l_s. It reflects that by propagating through N weakly scattering layers of tissue, the total phase accumulation is the sum of the phase shifts from each layer, as is typically assumed in phase imaging of transparent structures [10]. In essence, Eq. (1) describes the tissue *slice* angular scattering, while Eq. (3) characterizes the *bulk* tissue. The angular-scattering distribution, or phase function, $p(\theta)$ is obtained by performing azimuthal averaging of the scattering map, $p(\mathbf{q})$, associated with each tissue sample [Figs. 2(a)–2(c)]. The maximum scattering angle was determined by the NA of the objective lens and is about 18° for our current setup. The angular-scattering data were further fitted with Gegenbauer kernel (GK) phase function [16],

$$P(\theta) = ag\frac{(1-g^2)^{2a}}{\pi[1+g^2-2g\cos(\theta)]^{(a+1)}[(1+g)^{2a}-(1-g)^{2a}]}. \quad (4)$$

Note that g can be estimated directly from the angular-scattering data via its definition [Eq. (2)]. However, because of the limited angular range measured, g tends to be overestimated by this method, and thus the GK fit offers a more reliable alternative than the widely used Henyey–Greenstein (HG) phase function (with the parameter $a=1/2$). The representative fitting plots for each sample are shown in Figs. 3(d)–3(f). The final values of g are included in Fig. 3(b) and agree very well with previous reports in the literature [17].

From these measurements of thin singly scattering slices we inferred the behavior of light transport in thick strongly scattering tissue. Thus the transport mean-free path, which is the renormalized scattering length to account for the anisotropic phase function, can be obtained as $l^*=l_s/(1-g)$. The l^* values for 20 samples from each organ are shown in Fig. 3(c), which show larger standard deviations compared to l_s and g. These larger fluctuations are due to the combined effect of measuring both g and l_s.

In summary, we showed that FTLS can quantify the angular-scattering properties of thin tissues, which in turn provides the scattering mean-free path l_s and anisotropy factor g, for the macroscopic (bulk) organ. We note that based on the knowledge of l_s, g, and l^*, one can predict the outcome of a broad range of scattering experiments on large samples (size $\gg l^*$) via numerical solutions to the transport equation or analytical solutions to the diffusion equation. We envision that the FTLS measurements of unstained tissue biopsies, which are broadly available, will provide not only diagnosis value but also possibly the premise for a large scattering database, where various tissue types, healthy and diseased, will be fully characterized in terms of their scattering properties. At the opposite end of the spatial scales, FTLS can be used in combination with high-resolution microscopes to describe the angular (and dynamic) scattering of subcellular structures. For example, we have recently demonstrated that FTLS is sensitive to spatiotemporal organization of actin cytoskeleton [18]. Thus, FTLS can be used to study tissue optics from microscopic (organelle) to macroscopic (organ) spatial scales.

This research was supported in part by the National Science Foundation (NSF) (CAREER 08-46660) and the Grainger Foundation.

References

1. V. Backman, M. B. Wallace, L. T. Perelman, J. T. Arendt, R. Gurjar, M. G. Muller, Q. Zhang, G. Zonios, E. Kline, T. McGilligan, S. Shapshay, T. Valdez, K. Badizadegan, J. M. Crawford, M. Fitzmaurice, S. Kabani, H. S. Levin, M. Seiler, R. R. Dasari, I. Itzkan, J. Van Dam, and M. S. Feld, Nature **406**, 35 (2000).
2. R. Drezek, A. Dunn, and R. Richards-Kortum, Appl. Opt. **38**, 3651 (1999).
3. J. R. Mourant, M. Canpolat, C. Brocker, O. Esponda-Ramos, T. M. Johnson, A. Matanock, K. Stetter, and J. P. Freyer, J. Biomed. Opt. **5**, 131 (2000).
4. V. V. Tuchin, *Tissue Optics* (SPIE, 2000).
5. J. W. Pyhtila, K. J. Chalut, J. D. Boyer, J. Keener, T. D'Amico, M. Gottfried, F. Gress, and A. Wax, Gastrointest. Endosc. **65**, 487 (2007).
6. C. S. Mulvey, A. L. Curtis, S. K. Singh, and I. J. Bigio, IEEE J. Sel. Top. Quantum Electron. **13**, 1663 (2007).
7. H. Ding, J. Q. Lu, R. S. Brock, T. J. McConnell, J. F. Ojeda, K. M. Jacobs, and X. H. Hu, J. Biomed. Opt. **12**, 034032 (2007).
8. W. J. Cottrell, J. D. Wilson, and T. H. Foster, Opt. Lett. **32**, 2348 (2007).
9. H. Fang, L. Qiu, E. Vitkin, M. M. Zaman, C. Andersson, S. Salahuddin, L. M. Kimerer, P. B. Cipolloni, M. D. Modell, B. S. Turner, S. E. Keates, I. Bigio, I. Itzkan, S. D. Freedman, R. Bansil, E. B. Hanlon, and L. T. Perelman, Appl. Opt. **46**, 1760 (2007).
10. G. Popescu, in *Methods in Cell Biology*, P. J. Bhanu, ed. (Elsevier, 2008), Vol. 87.
11. F. Charriere, N. Pavillon, T. Colomb, C. Depeursinge, T. J. Heger, E. A. D. Mitchell, P. Marquet, and B. Rappaz, Opt. Express **14**, 7005 (2006).
12. W. Choi, C. Fang-Yen, K. Badizadegan, S. Oh, N. Lue, R. R. Dasari, and M. S. Feld, Nat. Methods **4**, 717 (2007).
13. W. Choi, C. C. Yu, C. Fang-Yen, K. Badizadegan, R. R. Dasari, and M. S. Feld, Opt. Lett. **33**, 1596 (2008).
14. G. Popescu, T. Ikeda, R. R. Dasari, and M. S. Feld, Opt. Lett. **31**, 775 (2006).
15. H. Ding, Z. Wang, F. Nguyen, S. A. Boppart, and G. Popescu, Phys. Rev. Lett. **101**, 238102 (2008).
16. L. O. Reynolds and N. J. Mccormick, J. Opt. Soc. Am. **70**, 1206 (1980).
17. J. M. Schmitt and G. Kumar, Appl. Opt. **37**, 2788 (1998).
18. H. Ding, L. J. Millet, M. U. Gillette, and G. Popescu, "Spatio-temporal cytoskeleton fluctuations probed by Fourier transform light scattering," submitted to Phys. Rev. Lett.
19. J. P. Ritz, A. Roggan, C. T. Germer, C. Isbert, G. Muller, and H. J. Buhr, Lasers Surg. Med. **28**, 307 (2001).
20. P. Parsa, S. L. Jacques, and N. S. Nishioka, Appl. Opt. **28**, 2325 (1989).